

Supplementary Information

Improvement of hydrothermal stability of zeolitic imidazolate frameworks

Xinlei Liu, Yanshuo Li, Yujie Ban, Yuan Peng, Hua Jin, Helge Bux,
Longya Xu, Jürgen Caro and Weishen Yang**

Table of contents

1. Preparation and evaluation experiments	S2
1.1 Preparation of ZIF-8 crystals with different methods	S2
1.2 Preparation of ZIF-7 and ZIF-93 nanoparticles	S2
1.3 Preparation of membranes and performance test	S2
1.4 Selective adsorption test cycles	S2
2. Characterizations	S5
XRD, SEM, TEM, IGA adsorption and diffusion measurements, FTIR-ATR, Raman spectra, Uv-vis absorption spectra, nitrogen physisorption measurements, ¹ HNMR, TG and contact angle measurements	S5
3. Results and discussion	S6
3.1 Hydrothermal test of ZIF-8, ZIF-7 and ZIF-93	S6
3.2 FTIR-ATR, photos, Raman spectra, Uv-vis absorption spectra and ¹ HNMR	S14
3.3 Shell-ligand-exchange-reaction (SLER) of ZIF-8 with different ligands	S19
3.4 N ₂ sorption isotherms and TG analysis	S20
3.5 Selective adsorption test cycles	S21
3.6 Performance of membranes	S22

1. Preparation and evaluation experiments

1.1 Preparation of ZIF-8 crystals with different methods

ZIF-8 nanocrystals (in methanol) were synthesized according to the route reported by Cravillon et al. ^[1] A solution of $\text{Zn}(\text{NO}_3)_2 \cdot 6\text{H}_2\text{O}$ (1.026 g, Aldrich, $\geq 99.0\%$) in 70 mL of methanol (BoDi, AR) was rapidly poured into a solution of MIM (2.072 g, Aldrich, 99%) in 70 ml of methanol under stirring at room temperature. After 1 h, the nanoparticles were separated from the mother liquid by centrifugation and washed with methanol for three times under ultrasonic.

ZIF-8 nanocrystals (in water) were synthesized according to the route reported by Pan et al. ^[2] A solution of $\text{Zn}(\text{NO}_3)_2 \cdot 6\text{H}_2\text{O}$ (1.69 g, Aldrich, $\geq 99.0\%$) in 11.56 g of deionized water was rapidly poured into a solution of MIM (32.79 g, Aldrich, 99%) in 115.6 g of deionized water under stirring at room temperature. After 5 min, the nanocrystals were separated from the mother liquid by centrifugation and washed with deionized water for two times under ultrasonic.

ZIF-8 microcrystals were synthesized in methanol according to the route reported by Bux et al. ^[3] A solution of 80 ml methanol (BoDi, AR) dissolved 1.08 g of zinc chloride (Aldrich, $\geq 98\%$), 0.97 g of MIM (Aldrich, 99%) and 0.54 g of sodium formate (BoDi, AR) was given into a 100 ml Teflon autoclave and heated in a microwave oven (MICROSYNTH, Milestone) at 100 °C for 4 h. After cooling, the microcrystals were separated from the mother liquid and washed with methanol for three times.

1.2 Preparation of ZIF-7 and ZIF-93 nanoparticles

ZIF-7 nanoparticles were prepared by a modified recipe reported by Li et al. ^[4] 750 mL N,N-dimethylformamide (BoDi, AR) was added into a solid mixture of 2.267 g $\text{Zn}(\text{NO}_3)_2 \cdot 6\text{H}_2\text{O}$ and 5.770 g benzimidazole (Aldrich, 98%) under stirring. After being kept at room temperature for 23 h, the product was centrifugally separated and washed with methanol. The SLER of ZIF-7 is the same as that of ZIF-8.

ZIF-93 ^[5] nanocrystals were firstly synthesized in this work. A solution of $\text{Zn}(\text{NO}_3)_2 \cdot 6\text{H}_2\text{O}$ (0.882 g, Aldrich, $\geq 99.0\%$) in 60 mL of methanol (BoDi, AR) was rapidly poured into a solution of 4-methylimidazole-5-carbaldehyde (2.610 g, Aldrich, 99%) in 60 mL of methanol under stirring at room temperature. After 20 min, the nanoparticles were separated from the mother liquid by centrifugation and washed with ethanol for three times under ultrasonic. The yield is about 40% based on zinc. As shown in Figure S19, the XRD pattern of this material is consistent with that reported by Yaghi et al. ^[5] indicates the ZIF-93

was successfully prepared. The size of ZIF-93 is around 40 nm. The SLER of ZIF-93 is the same as that of ZIF-8.

1.3 Preparation of membranes and performance test

The ZIF-8-DMBIM-PMPS membrane was prepared using the same solution-blending method as that of the ZIF-8-PMPS membrane except that the ZIF-8-DMBIM was used instead of ZIF-8. ^[6] Alumina capillary tubes (3.7 mm OD, 2.4 mm ID, 6.0 cm length, Hyflux Ltd.) were used as supports. The pore size of the inner surface was 40 nm. The as-synthesized ZIF-8-DMBIM nanoparticles were re-dispersed in i-octane (Kermel, AR) using a probe-type sonicator (AiDaPu) with the horn immersed in the sample for 10 minutes in an ice bath. This solution (4.5 wt. %) was then allowed to heat to room temperature. The catalyst (dibutyltin dilaurate, Shanghai Resin Factory Co., Ltd.), curing agent (Tetraethyl orthosilicate, Kermel, AR), i-octane, PMPS (Shanghai Resin Factory Co., Ltd.) and the above ZIF-8-DMBIM i-octane solution were added to a glass bottle one after another to give the weight composition: Catalyst / TEOS / PMPS / ZIF-8-DMBIM / i-octane = 1 : 10 : 100 : 10 : 333. This mixture was sonicated for 5 minutes using a probe-type sonicator in an ice bath. The resulting homogeneous mixture was then kept at room temperature for 10 minutes. Then, the capillary tube was dip-coated into this mixture for 10 s and withdrawn at a speed of 1 mm / s using an automatic dip-coator (WPTL0.01). The membrane was cured at 25 °C for 24 h, 100 °C for 12 h and then kept at 100 °C for another 12 h under vacuum.

The operating details and apparatus of the membrane performance test were shown previously. ^[6] The feed mixtures (ca. 2.0 L) for pervaporation experiments were kept at 45-80 °C with a composition of 1.0-3.0 wt. % isobutanol. To minimize the boundary layer effect on the membrane surface, the feed flow rate was kept sufficiently high (2.0 L / min). After circling 10 min for stabilization, the pervaporation performance was characterized. The permeation side was kept under vacuum and the permeate was trapped with liquid nitrogen. The permeation flux was measured by weighing the condensed permeate:

$$J = W/(A \cdot t)$$

where W refers to the weight of permeate (kg), A the membrane area (m²), t the duration (h) of the sample collection. The feed and permeate concentrations were measured by an off-line GC (Agilent 7890). In most cases for separating isobutanol from water, the condensed permeate separated into two phases. In order to measure the concentration in the condensate, the permeate was diluted with known quantity of water to generate a single phase.

1.4 Selective adsorption test cycles

Selective adsorption cycles test of isobutanol from water: I) preliminary treatment: 0.120g of ZIF-8 (or ZIF-8-DMBIM) samples (previously dried at 80 °C under vacuum for 24h) immersed in 200g of 3.0 wt. % isobutanol aqueous solution ($W_{\text{crystals}} / (W_{\text{crystals}} + W_{\text{aqueous solution}}) = 0.060$ wt. %) were sealed in a glass bottle and heated at 80 °C in a convection oven for 24h. Afterwards, the samples were collected and dried at 80 °C for 24 h under vacuum. Preliminary experiments were performed to conclude that the physically adsorbed molecules in the frameworks can be completely desorbed at these conditions. [6] The samples were characterized by the XRD. II) Selective adsorption of isobutanol from water using solution-depletion method: [7] 0.020 g of samples from I) were immersed in 1.000g of 3.0 wt. % isobutanol aqueous solution and sealed for 5h under swag at 25 °C. Preliminary experiments were performed for various adsorption times to conclude that 5 h was long enough for the adsorption to reach equilibrium. A blank was subjected to the procedure to correct for any change of the adsorbate. After the centrifugation, a clear supernatant came forth and its concentration was estimated using gas chromatography (GC, Agilent 7890). The uptake was determined using the mass balance equation

$$Q = M (C_i - C_e) / m,$$

where Q is the amount adsorbed by the samples at equilibrium (mg / g), M is the mass of solution used in the adsorption experiment (mg), C_i and C_e are the initial and equilibrium mass concentrations of isobutanol, respectively, and m is the mass of samples (g).

[1] J. Cravillon, S. Munzer, S. J. Lohmeier, A. Feldhoff, K. Huber, M. Wiebcke, *Chem. Mater.*, 2009, **21**, 1410.

[2] Y. Pan, Y. Liu, G. Zeng, L. Zhao, Z. Lai, *Chem. Commun.*, 2011, 47, 2071.

[3] H. Bux, F. Liang, Y. Li, J. Cravillon, M. Wiebcke, J. Caro, *J. Am. Chem. Soc.*, 2009, 131, 16000.

[4] Y. S. Li, F. Y. Liang, H. Bux, A. Feldhoff, W. S. Yang, J. Caro, *Angew. Chem. Int. Ed.*, 2010, **49**, 548.

[5] W. Morris, B. Leung, H. Furukawa, O. K. Yaghi, N. He, H. Hayashi, Y. Houndonougbo, M. Asta, B. B. Laird, O. M. Yaghi, *J. Am. Chem. Soc.*, 2010, **132**, 11006.

[6] X. L. Liu, Y. S. Li, G. Q. Zhu, Y. J. Ban, L. Y. Xu, W. S. Yang, *Angew. Chem. Int. Ed.* 2011, **50**, 10636.

[7] R. Ranjan, S. Thust, C. E. Gounaris, M. Woo, C. A. Floudas, M. v. Keitz, K. J. Valentas, J. Wei, M. Tsapatsis, *Micropor. Mesopor. Mater.*, 2009, **122**, 143.

2. Characterizations

XRD (x-ray diffraction) patterns were recorded on Rigaku D/MAX 2500/PC (using Cu K α radiation, $\lambda=0.154$ nm at 40kV and 200mA). The SEM (Scanning Electron Microscope) images were performed on a Quanta 200 FEG instrument (FEI Co.). The samples were sputter coated with gold before characterization. The TEM (Transmission Electron Microscope) images were performed on a Tecnai G2 Spirit instrument (FEI Co.).

The adsorption studies were carried out gravimetrically in an Intelligent Gravimetric Analyzer (IGA-002/3). The adsorbents were activated by heating to 100 °C and then tested at 40 °C by accurately controlling the pressure of vapor. The transient and equilibrium weight changes of the samples were measured and recorded for analysis. The transport diffusivity was determined based on the Fick's second law assuming the samples as spherical particles (see the following equation):

$$\frac{A_t - A_0}{A_\infty - A_0} = 1 - \frac{6}{\pi^2} \sum_{n=1}^{\infty} \frac{1}{n^2} \exp\left(-\frac{n^2 \pi^2 D t}{r^2}\right)$$

where D, r, t denote the transport diffusivity, radius of particle and time, respectively. A_0 , A_t , A_∞ are the uptake at time 0, t, ∞ , respectively.

Infrared spectra were acquired from a Nicolet 6700 FTIR-ATR (Fourier Transform Infrared Spectroscopy-Attenuated Total Reflectance) spectrophotometer. Raman spectra were acquired from T64000 (Horiba Jobin Yvon) and inVia (Renishaw) microscopes using 325 and 514 nm exciting laser wavelength, respectively. Uv-vis absorption spectra were acquired from a JASCO V-550 spectrophotometer. Nitrogen physisorption isotherms were measured at 77 K, on a Quantachrome Autosorb Automated Gas Sorption instrument. For comparison, the ZIF-8 nanocrystals was washed one time at 60 °C after washed at room temperature in methanol.

The ^1H NMR (Nuclear Magnetic Resonance) spectra were recorded on a Bruker AVANCE III 400 MHz (SB) spectrometer at room temperature. A minimum of 35wt. % $\text{DCI}/\text{D}_2\text{O}$ was used to digest the crystals, while DMSO-d_6 and CDCl_3 were used for solvent. For TG (Thermogravimetry) analysis, the samples were heated in a flow of air with a ramp of 10 °C / min on a Pyris Diamond instrument. The water droplet contact angle measurements were carried out at room temperature with 5 μL water droplet on the packing of sample using a system JC 2000A. The contact angle values reported are averages of three measurements made on different positions of the sample surface and all measurements are within $\pm 2^\circ$ of the averages. The packing is done in an identical way in each experiment in order to get comparable results.

3. Results and discussion

3.1 Hydrothermal test of ZIF-8, ZIF-7 and ZIF-93

Figure S1.

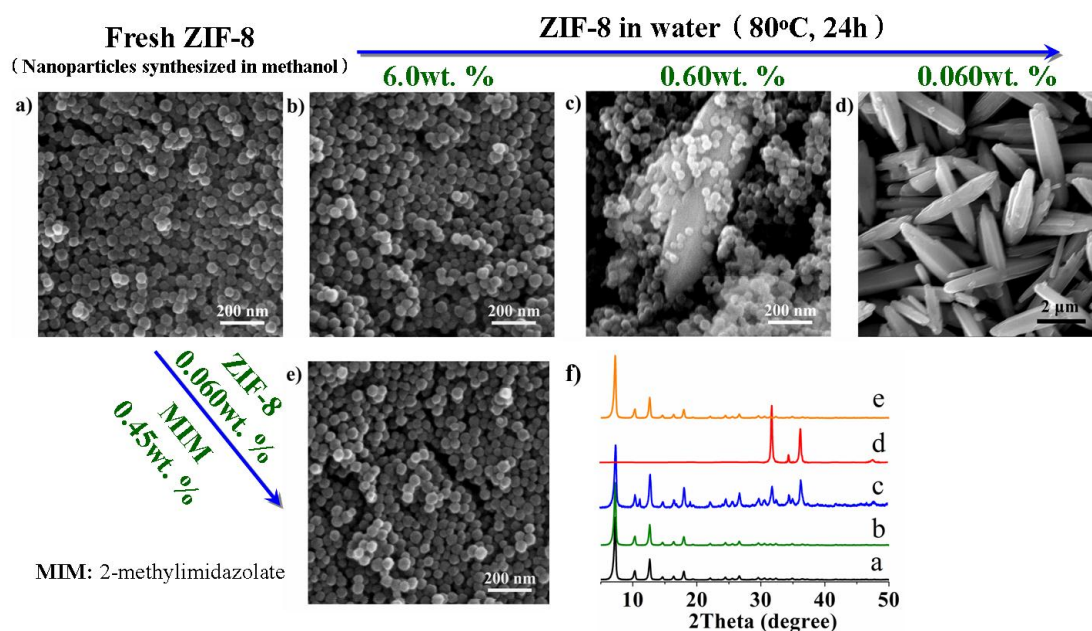


Figure S1. SEM images of a) the ZIF-8 nanocrystals (synthesized in methanol); the ZIF-8 sample after hydrothermal test in 80 °C water for 24h at a high crystal concentration ($W_{\text{ZIF-8}} / (W_{\text{ZIF-8}} + W_{\text{water}}) = 6.0 \text{ wt. \%}$) (b)), at a middle crystal concentration (0.60 wt. %) (c)), at a low crystal concentration (0.060 wt. %) (d)) and at a low crystal concentration (0.060 wt. %) but additional ligands (MIM) were previously dissolved in the water ($W_{\text{MIM}} / (W_{\text{MIM}} + W_{\text{water}}) = 0.45 \text{ wt. \%}$) (e)); f) the XRD patterns of the samples corresponding to a) (black), b) (olive), c) (blue), d) (red) and e) (orange).

As shown in Figure S1, the ZIF-8 nanocrystals (synthesized in methanol) are unperturbed after hydrothermal test in hot water (80 °C, 24h) employing a high crystal concentration (6.0 wt. %). This phenomenon is consistent with former literature reports.^[1-3] Nevertheless, a gradual decomposition of ZIF-8 was shown to accelerate with the decreasing crystal concentration. At a low crystal concentration (0.060 wt. %), the ZIF-8 crystals were completely transformed into ZnO as proved by the SEM and XRD characterizations. When amount of ligands stuff (MIM) of ZIF-8 were previously dissolved in the water ($W_{\text{MIM}} / (W_{\text{MIM}} + W_{\text{water}}) = 0.45 \text{ wt. \%}$), the decomposition of ZIF-8 was successfully restrained. From another side, the above phenomena indicate that the reason why the ZIF-8 is stable in water (liquid or steam) at high crystal concentration is based on the protection of its released ligands

in water, which come from the residuals on the ZIF-8 and (or) few early decomposed ZIF-8. The bare ZIF-8 itself is not stable in water at 80 °C.

[1] K. S. Park, Z. Ni, A. P. Côté, J. Y. Choi, R. Huang, F. J. Uribe-Romo, H. K. Chae, M. O'Keeffe, O. M. Yaghi, *Proc. Natl. Acad. Sci.*, 2006, **103**, 10186.

[2] Y. Pan, Y. Liu, G. Zeng, L. Zhao, Z. Lai, *Chem. Commun.*, 2011, **47**, 2071.

[3] J. J. Low, A. I. Benin, P. Jakubczak, J. F. Abrahamian, S. A. Faheem, R. R. Willis, *J. Am. Chem. Soc.*, 2009, **131**, 15834.

Figure S2.

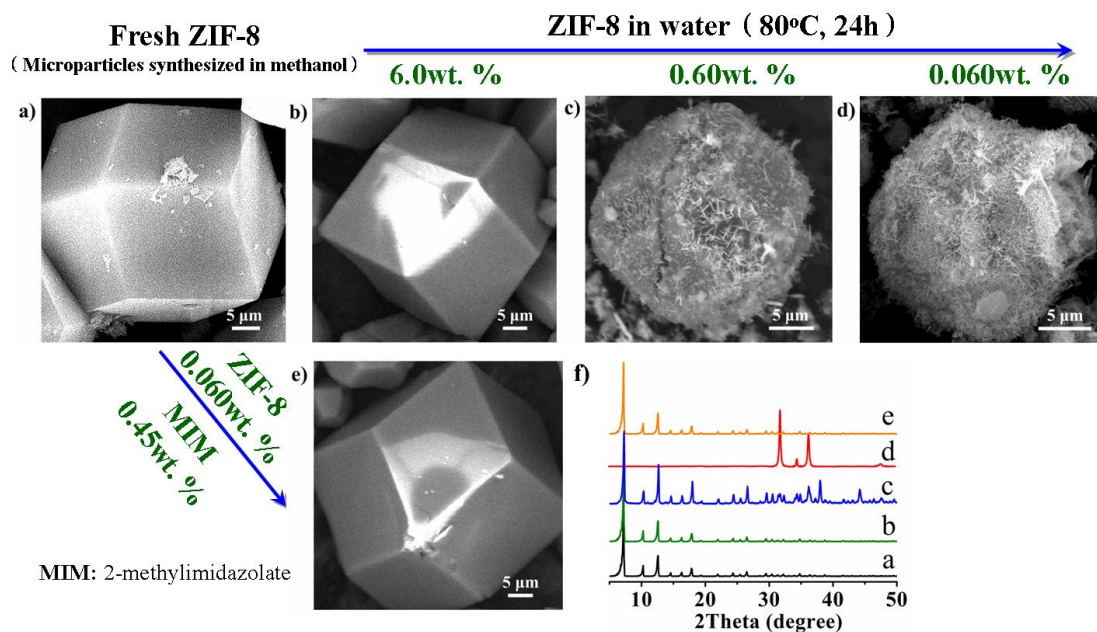


Figure S2. SEM images of a) the ZIF-8 microcrystals (synthesized in methanol); the ZIF-8 sample after hydrothermal test in 80 °C water for 24h at a high crystal concentration ($W_{\text{ZIF-8}} / (W_{\text{ZIF-8}} + W_{\text{water}}) = 6.0 \text{ wt. \%}$) (b)), at a middle crystal concentration (0.60 wt. %) (c)), at a low crystal concentration (0.060 wt. %) (d)) and at a low crystal concentration (0.060 wt. %) but additional ligands (MIM) were previously dissolved in the water ($W_{\text{MIM}} / (W_{\text{MIM}} + W_{\text{water}}) = 0.45 \text{ wt. \%}$) (e)); f) the XRD patterns of the samples corresponding to a) (black), b) (olive), c) (blue), d) (red) and e) (orange).

As shown in Figure S2, the ZIF-8 microcrystals (synthesized in methanol) are unperturbed after hydrothermal test in hot water (80 °C, 24h) employing a high crystal concentration (6.0 wt. %). This phenomenon is consistent with former literature reports.^[1-3] Nevertheless, a gradual decomposition of ZIF-8 was shown to accelerate with the decreasing crystal concentration. At a low crystal concentration (0.060 wt. %), the ZIF-8 crystals were completely transformed into ZnO as proved by the SEM and XRD characterizations. When amount of ligands stuff (MIM) of ZIF-8 were previously dissolved in the water ($W_{\text{MIM}} / (W_{\text{MIM}} + W_{\text{water}}) = 0.45 \text{ wt. \%}$), the decomposition of ZIF-8 was successfully restrained. From another side, the above phenomena indicate that the reason why the ZIF-8 is stable in water (liquid or steam) at high crystal concentration is based on the protection of its released ligands in water, which come from the residuals on the ZIF-8 and (or) few early decomposed ZIF-8. The bare ZIF-8 itself is not stable in water at 80 °C.

- [1] K. S. Park, Z. Ni, A. P. Côté, J. Y. Choi, R. Huang, F. J. Uribe-Romo, H. K. Chae, M. O’Keeffe, O. M. Yaghi, *Proc. Natl. Acad. Sci.*, 2006, **103**, 10186.
- [2] Y. Pan, Y. Liu, G. Zeng, L. Zhao, Z. Lai, *Chem. Commun.*, 2011, **47**, 2071.
- [3] J. J. Low, A. I. Benin, P. Jakubczak, J. F. Abrahamian, S. A. Faheem, R. R. Willis, *J. Am. Chem. Soc.*, 2009, **131**, 15834.

Figure S3.

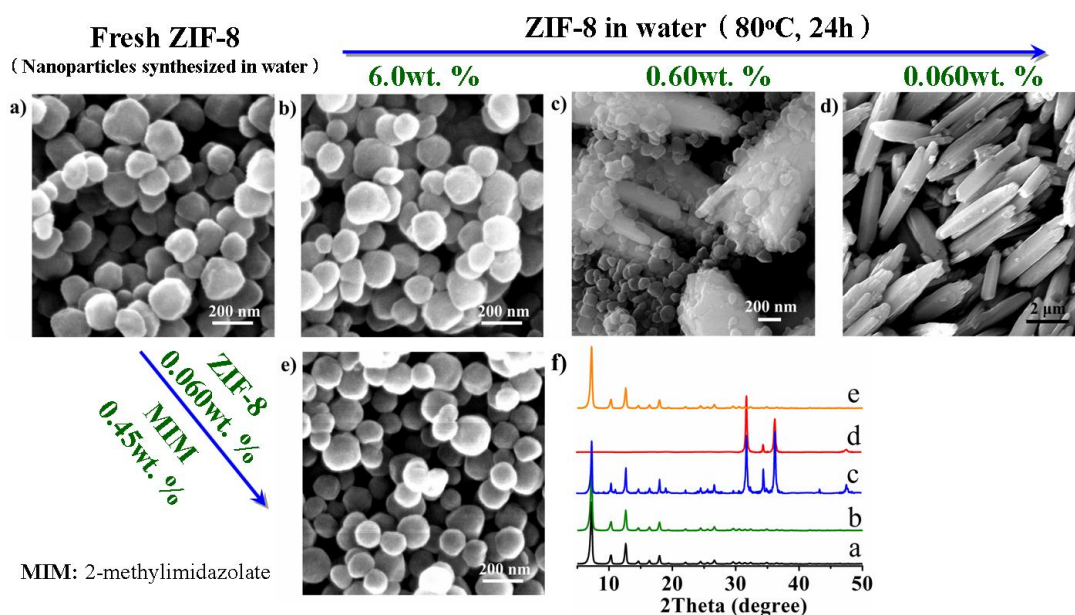


Figure S3. SEM images of a) the ZIF-8 nanocrystals (synthesized in water); the ZIF-8 sample after hydrothermal test in 80 °C water for 24h at a high crystal concentration ($W_{\text{ZIF-8}} / (W_{\text{ZIF-8}} + W_{\text{water}}) = 6.0 \text{ wt. } \%$) (b)), at a middle crystal concentration (0.60 wt. %) (c)), at a low crystal concentration (0.060 wt. %) (d)) and at a low crystal concentration (0.060 wt. %) but additional ligands (MIM) were previously dissolved in the water ($W_{\text{MIM}} / (W_{\text{MIM}} + W_{\text{water}}) = 0.45 \text{ wt. } \%$) (e)); f) the XRD patterns of the samples corresponding to a) (black), b) (olive), c) (blue), d) (red) and e) (orange).

As shown in Figure S3, the ZIF-8 nanocrystals (synthesized in water) are unperturbed after hydrothermal test in hot water (80 °C, 24h) employing a high crystal concentration (6.0 wt. %). This phenomenon is consistent with former literature reports.^[1-3] Nevertheless, a gradual decomposition of ZIF-8 was shown to accelerate with the decreasing crystal concentration. At a low crystal concentration (0.060 wt. %), the ZIF-8 crystals were completely transformed into ZnO as proved by the SEM and XRD characterizations. When amount of ligands stuff (MIM) of ZIF-8 were previously dissolved in the water ($W_{\text{MIM}} / (W_{\text{MIM}} + W_{\text{water}}) = 0.45 \text{ wt. } \%$), the decomposition of ZIF-8 was successfully restrained. From another side, the above phenomena indicate that the reason why the ZIF-8 is stable in water (liquid or steam) at high crystal concentration is based on the protection of its released ligands in water, which come from the residuals on the ZIF-8 and (or) few early decomposed ZIF-8. The bare ZIF-8 itself is not stable in water at 80 °C.

[1] K. S. Park, Z. Ni, A. P. Côté, J. Y. Choi, R. Huang, F. J. Uribe-Romo, H. K. Chae, M. O’Keeffe, O. M. Yaghi, *Proc. Natl. Acad. Sci.*, 2006, **103**, 10186.

[2] Y. Pan, Y. Liu, G. Zeng, L. Zhao, Z. Lai, *Chem. Commun.*, 2011, **47**, 2071.

[3] J. J. Low, A. I. Benin, P. Jakubczak, J. F. Abrahamian, S. A. Faheem, R. R. Willis, *J. Am. Chem. Soc.*, 2009, **131**, 15834.

Figure S4.

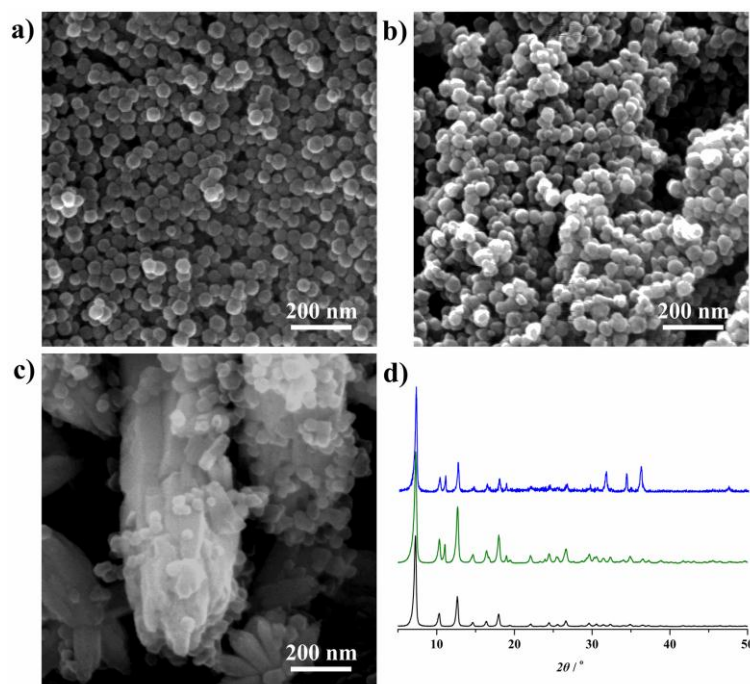


Figure S4. SEM images of a) the ZIF-8 nanocrystals (synthesized in methanol); the ZIF-8 sample after hydrothermal test in water for 24h with a low crystal concentration ($W_{\text{ZIF-8}} / (W_{\text{ZIF-8}} + W_{\text{water}}) = 0.060$ wt. %) at 25 °C (b)) and 50 °C (c)); d) the XRD patterns of the samples corresponding to a) (black), b) (olive) and c) (blue).

As shown in Figure S4, the ZIF-8 nanocrystals (synthesized in methanol) are not stable in water with a low crystal concentration even at 50 °C and 25 °C.

Figure S5.

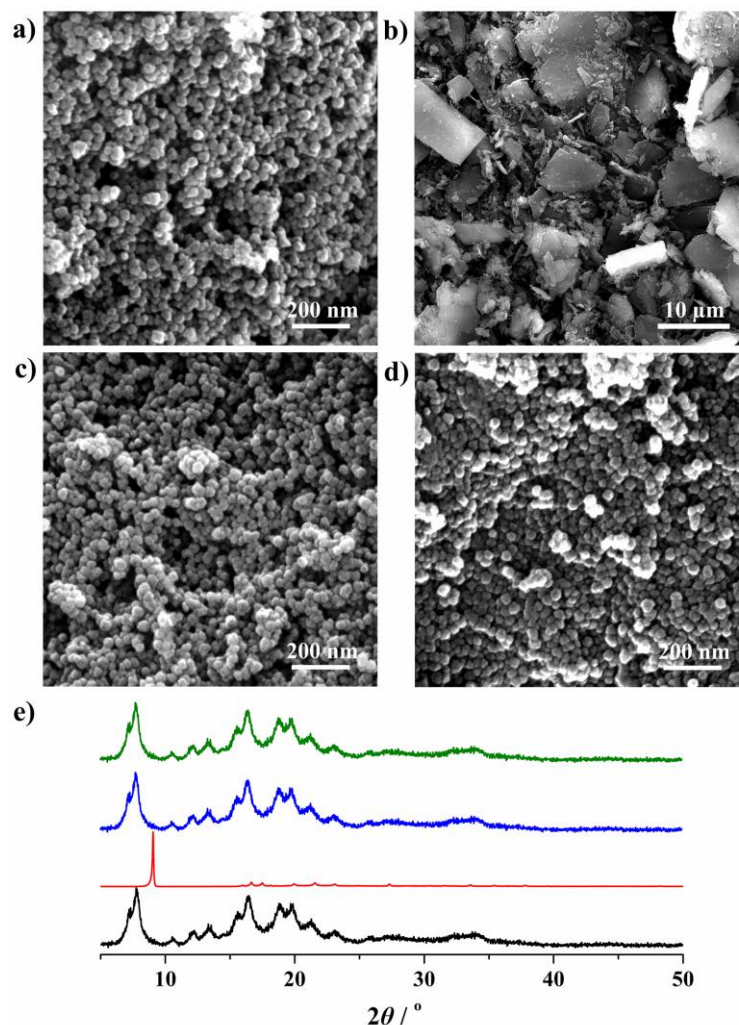


Figure S5. SEM images of a) the as-synthesized ZIF-7 nanocrystals; b) the ZIF-7 sample after hydrothermal test in 80 °C water for 24h at a low crystal concentration ($W_{\text{ZIF-7}} / (W_{\text{ZIF-7}} + W_{\text{water}}) = 0.060$ wt. %); c) the ZIF-7 after SLER (termed as ZIF-7-DMBIM); d) the ZIF-7-DMBIM sample after hydrothermal test in 80 °C water for 24h at a low crystal concentration (0.060 wt. %); e) the XRD patterns of the samples corresponding to a) (black), b) (red), c) (blue) and d) (olive).

The ZIF-7 nanoparticles were completely destroyed after the hydrothermal test. After the SLER, the decomposition of ZIF-7 nanocrystals was successfully restrained. This confirms the general applicability of this method.

Figure S6.

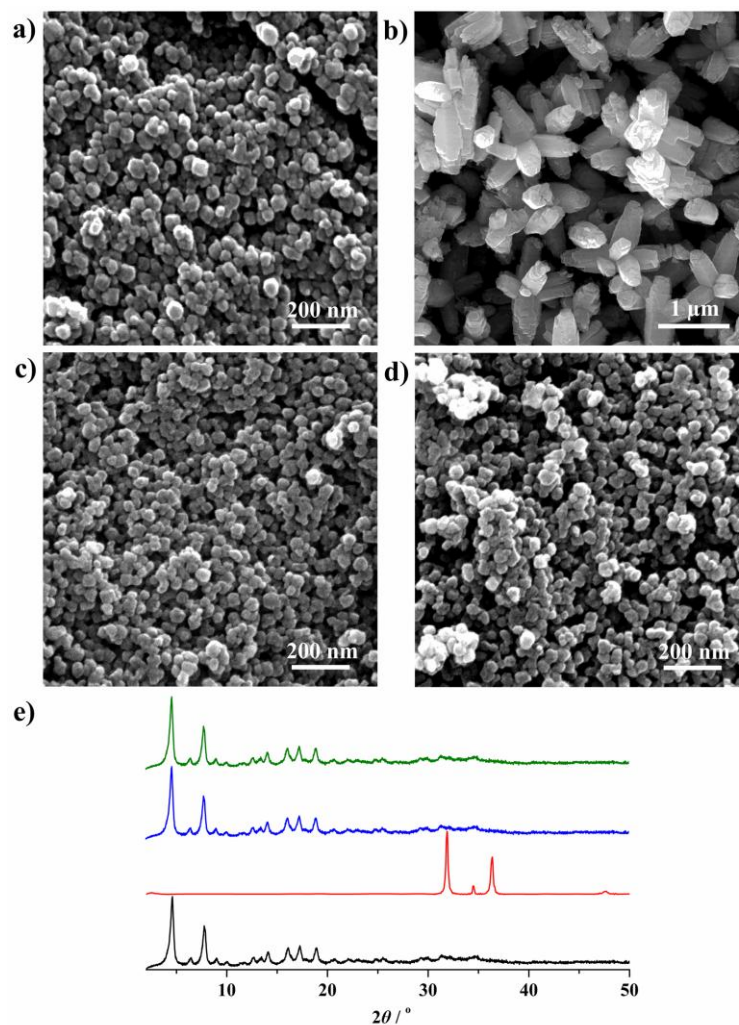


Figure S6. SEM images of a) the as-synthesized ZIF-93 nanocrystals; b) the ZIF-93 sample after hydrothermal test in 80 °C water for 24h at a low crystal concentration ($W_{\text{ZIF-93}} / (W_{\text{ZIF-93}} + W_{\text{water}}) = 0.060$ wt. %); c) the ZIF-93 after SLER (termed as ZIF-93-DMBIM); d) the ZIF-93-DMBIM sample after hydrothermal test in 80 °C water for 24h at a low crystal concentration (0.060 wt. %); e) the XRD patterns of the samples corresponding to a) (black), b) (red), c) (blue) and d) (olive).

The ZIF-93 nanoparticles were completely destroyed after the hydrothermal test. After the SLER, the decomposition of ZIF-93 nanocrystals was successfully restrained. This confirms the general applicability of this method.

3.2 FTIR-ATR, Raman spectra, photos, Uv-vis absorption spectra and ^1H NMR

Figure S7.



Figure S7. Photos of ZIF-8 and ZIF-8-DMBIM nanocrystals in weighing bottles.

After the SLER, the color of the ZIF-8 powder changed into slightly beige even after exhaustive washing, which is the same as that of the DMBIM ligands, implying the deprotonation of DMBIM and subsequent coordination of imidazole nitrogen to zinc ions.

Figure S8.

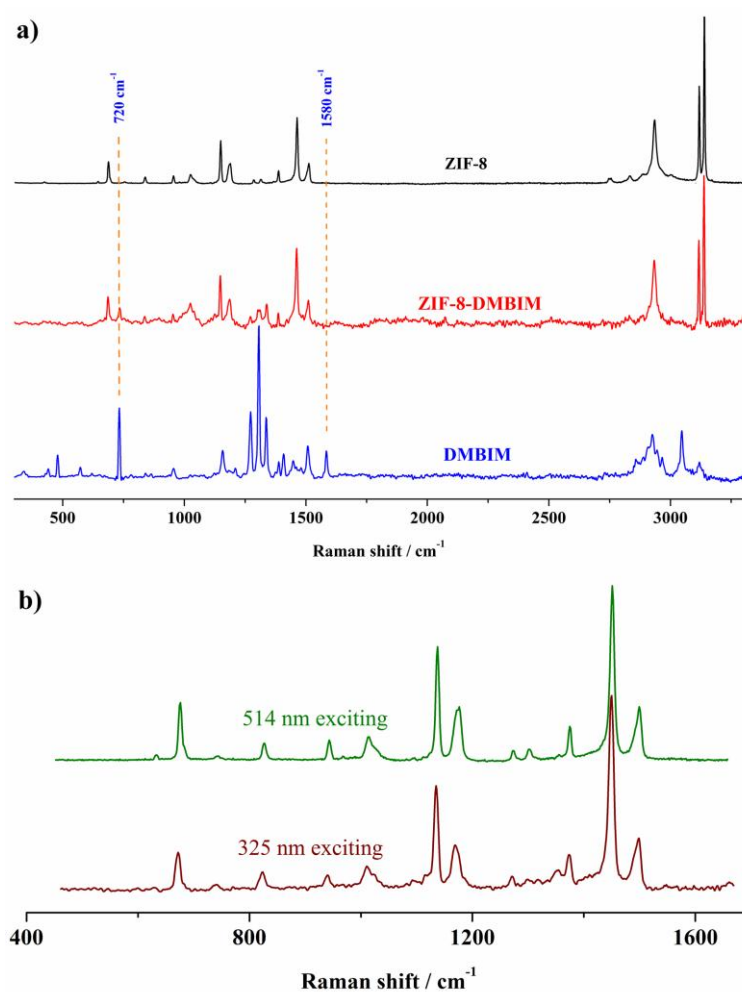


Figure S8. a) Raman spectra of the DMBIM (blue), ZIF-8 (black) and ZIF-8-DMBIM (red) nanoparticles using 514 nm exciting laser wavelength; b) Raman spectra of ZIF-8 nanoparticles using different exciting laser wavelength (olive: 514 nm; wine: 325 nm).

In the Raman spectra (Figure S8a), the presentation of the new additional peaks at 720 cm^{-1} , corresponding to the in-plane deformation vibrations of the fused ring of DMBIM, and the disappearance of the peak at 1580 cm^{-1} , corresponding to the N-H bending vibrations, confirms the existence and deprotonation of DMBIM in ZIF-8-DMBIM, and thus the efficiency of the ligand exchange. No influence of the Raman spectra of the ZIF-8 nanocrystals takes place when the exciting wavelength changes from 514 nm to 325 nm (Figure S8b) demonstrates that the structure of ZIF-8 is homogeneous.

Figure S9.

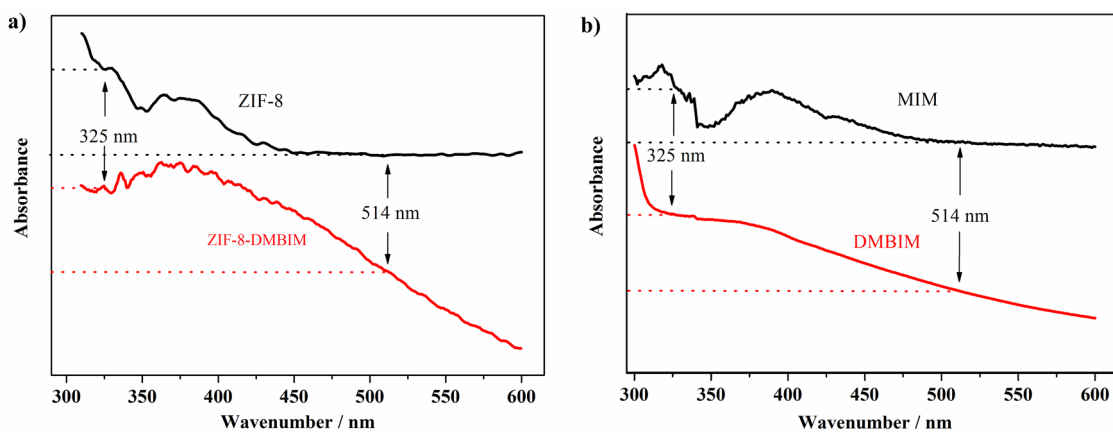


Figure S9. UV-vis absorption spectra of a) ZIF-8 (black) and ZIF-8-DMBIM (red) nanocrystals and b) MIM (black) and DMBIM (red) powders.

For ZIF-8, ZIF-8-DMBIM, MIM and DMBIM, the penetration depth is directly proportional to the exciting wavelength (325 nm vs. 514 nm) because of decreased absorbance.

Figure S10.

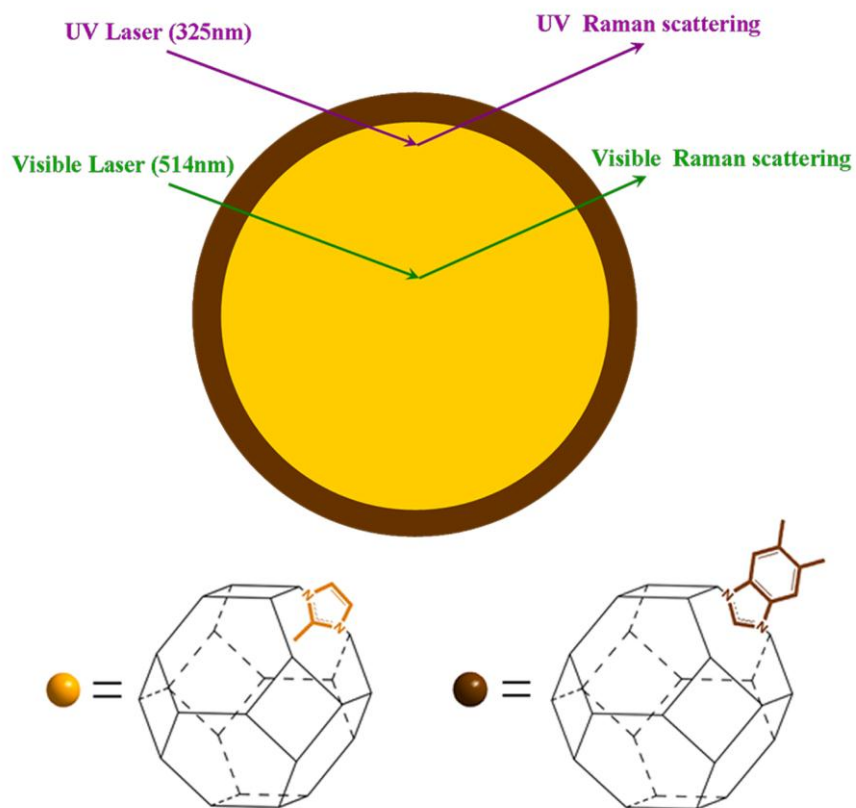


Figure S10. Schematic representations of the structure of ZIF-8-DMBIM and its Raman scattering with different laser excitation sources.^[1]

[1] M. Li, Z. Feng, G. Xiong, P. Ying, Q. Xin, C. Li, *J. Phys. Chem. B*, 2001, **105**, 8107.

Figure S11.

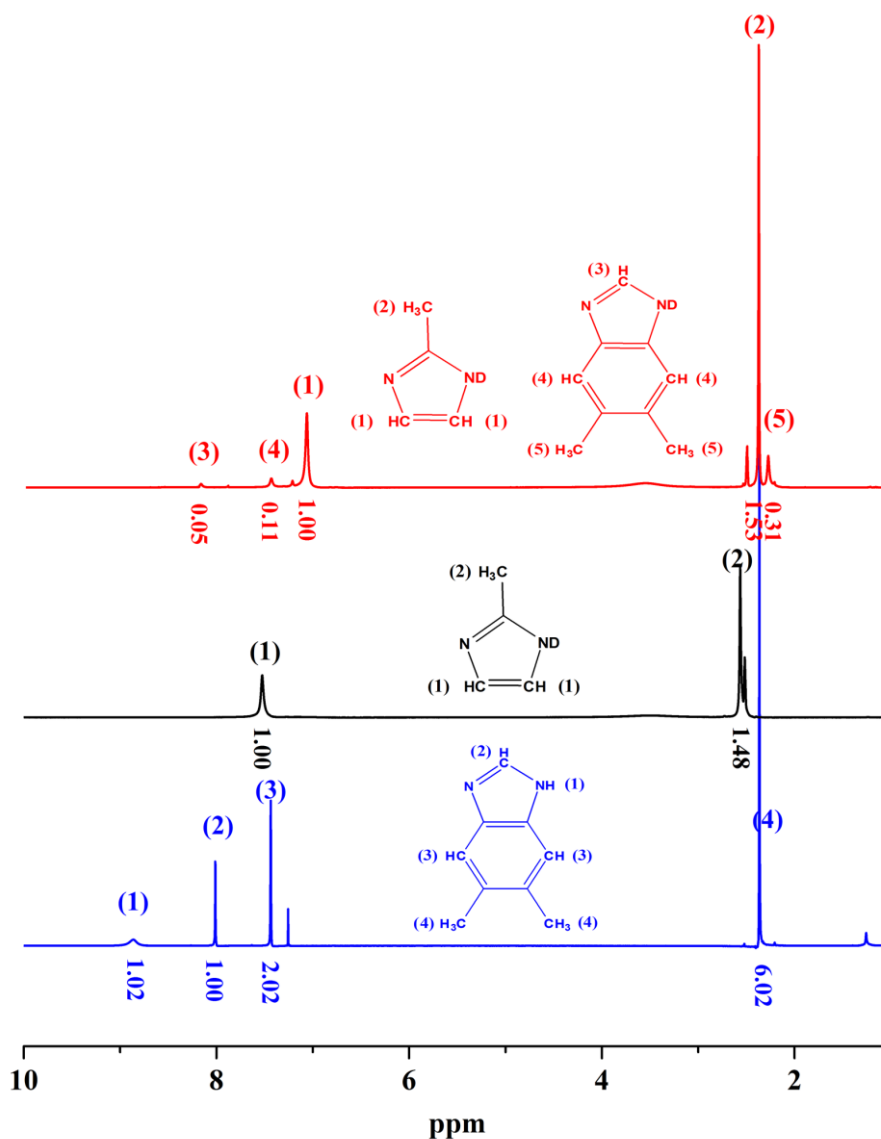


Figure S11. The ¹H NMR spectra of the dissolved 5,6-dimethylbenzimidazole (DMBIM, blue), digested ZIF-8 (black) and ZIF-8-DMBIM (red). The numbers on the top of the peaks, corresponding to the numbers of the molecular formula, represent different types of proton signals. The numbers under the peaks are the relative integration.

As shown in Figure S11, a 9.1% ($M_{\text{DMBIM}} / (M_{\text{DMBIM}} + M_{\text{MIM}})$) ligand exchange molar ratio is identified based on the signal integration of ¹H NMR.

3.3 Shell-ligand-exchange-reaction of ZIF-8 with different ligands

Figure S12.

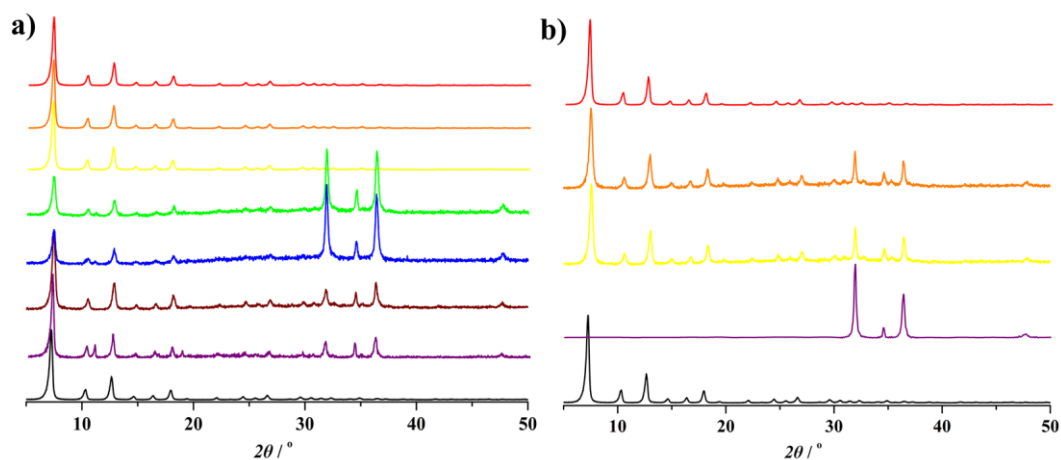


Figure S12. XRD patterns of ZIF-8-DMBIM (red), ZIF-8-BIM (orange), ZIF-8-MTFMIM (yellow), ZIF-8-IPIM (green), ZIF-8-EIM (blue), ZIF-8-TFMIM (wine) and ZIF-8 (purple) after hydrothermal test in water with a low crystal concentration (0.060 wt. %) at 50 °C (a) and 80 °C (b) for 24h. The XRD patterns of the as-synthesized ZIF-8 nanocrystals (black) are shown for reference.

Imidazole derivatives (2-methyl-4-trifluoromethylimidazole (MTFMIM), 4-trifluoromethylimidazole (TFMIM), 2-ethylimidazole (EIM), 2-isopropylimidazole (IPIM) and benzimidazole (BIM)) containing different hydrophobic groups were used to substitute MIM ligands from ZIF-8 nanocrystals employing the same SLER as that of DMBIM. All the XRD patterns of the ZIF-8 after SLER were not changed (not shown here). Combined with the XRD characterization (Figure S12), the structures of ZIF-8-IPIM, ZIF-8-EIM, ZIF-8-TFMIM and ZIF-8 changed after hydrothermal test in water at 50 °C, while that of ZIF-8-DMBIM, ZIF-8-BIM and ZIF-8-MTFMIM are retained. At 80 °C, the ZIF-8-BIM and ZIF-8-MTFMIM were partly decomposed with an unperturbed ZIF-DMBIM. This indicates that the imidazole derivatives substitutes possessing various hydrophobic groups can give different enhancement of water resistant to ZIF-8.

3.4 N₂ sorption isotherms and TG analysis

Figure S13.

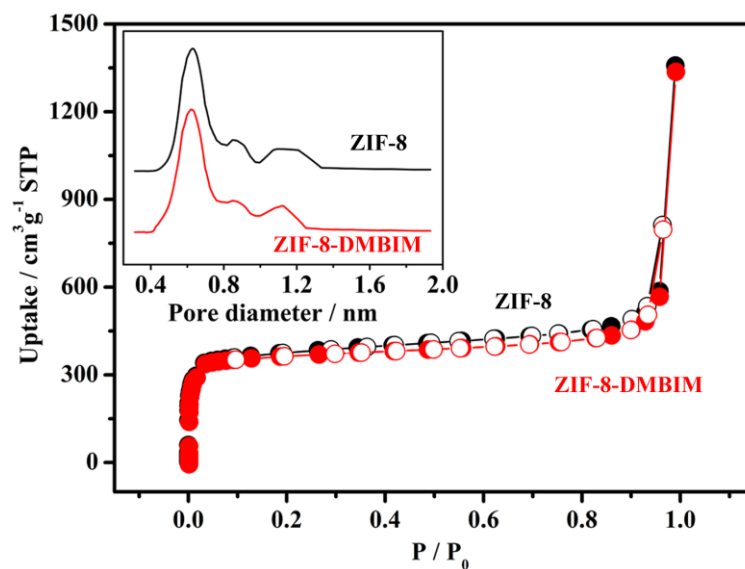


Figure S13. The N₂ sorption isotherms (77K) and (inset) pore size analysis (Hovarth-Kawazoe method) of ZIF-8 (black) and ZIF-8-DMBIM (red).

Only a negligible decrease in BET surface area (from 1360 to 1346 m²/g) and pore volume (from 0.572 to 0.567 cm³/g) was observed after SLER. There is no distinct difference of the pore size distribution between ZIF-8-DMBIM and ZIF-8.

Figure S14.

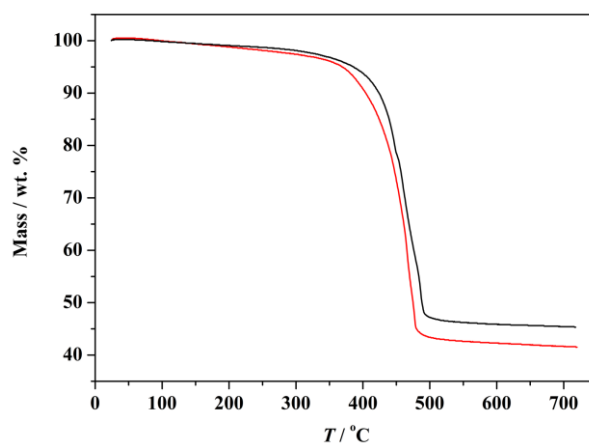


Figure S14. TG curves for ZIF-8 (black) and ZIF-8-DMBIM (red) nanocrystals measured in a flow of air. The TG curve of ZIF-8-DMBIM is consistent with that of ZIF-8.

3.5 Selective adsorption test cycles

Figure S15.

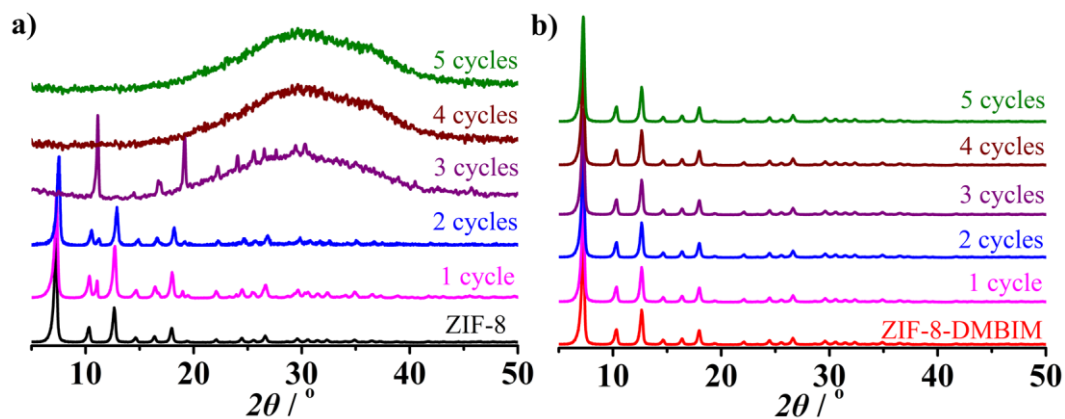


Figure S15. XRD patterns of ZIF-8 (a) and ZIF-8-DMBIM (b)) after hydrothermal test for different cycles for the selective adsorption of isobutanol from water, the XRD patterns of the as-synthesized ZIF-8 and ZIF-8-DMBIM are shown for reference.

As shown in Figure S15, the structure of ZIF-8 was completely destroyed after four cycles while that of ZIF-8-DMBIM remains essentially unchanged even after five cycles.

3.6 Performance of membranes

Figure S16.

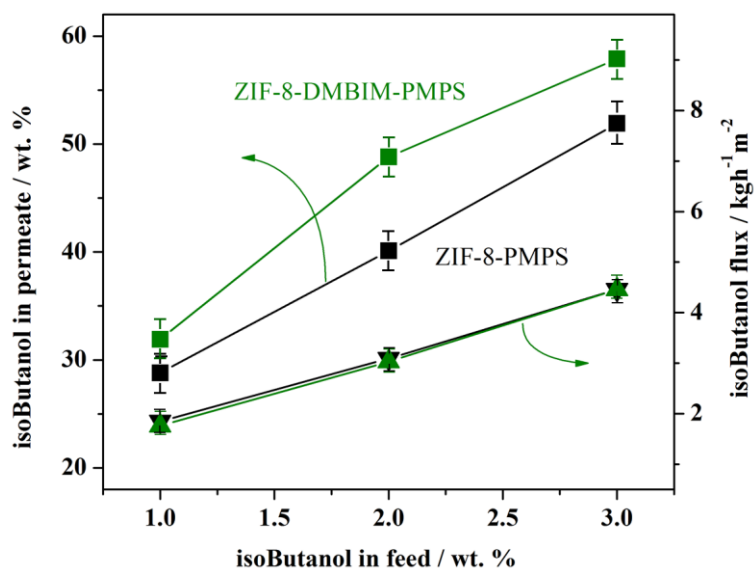


Figure S16. isoButanol concentration in permeate (squares) and isobutanol flux (triangles) as function of feed concentration (upstream side, 80 °C) for ZIF-8 (black) and ZIF-8-DMBIM (olive) derived mixed matrix membranes.

Compared with ZIF-8-PMPS membrane, the ZIF-8-DMBIM-PMPS membrane exhibited improved selectivity towards isobutanol while keeping the isobutanol flux (productivity) constant.

Figure S17.

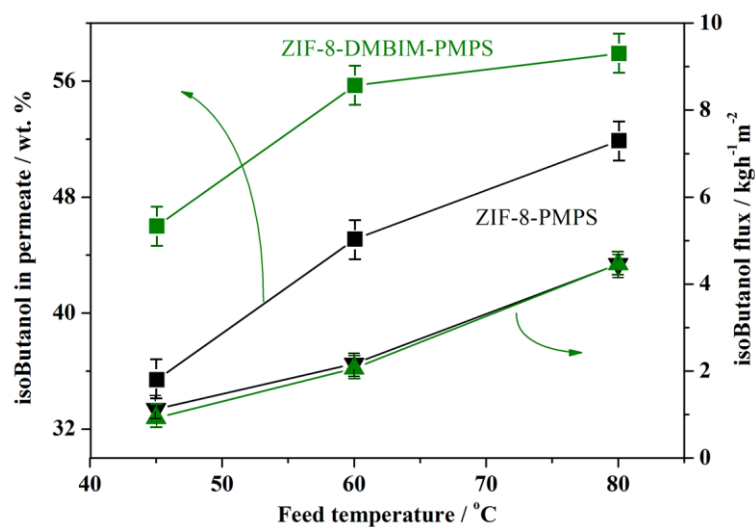


Figure S17. isoButanol concentration in permeate (squares) and isobutanol flux (triangles) as function of feed temperature (upstream side, 3.0 wt. % isobutanol) for ZIF-8 (black) and ZIF-8-DMBIM (olive) derived mixed matrix membranes.

Compared with ZIF-8-PMPS membrane, the ZIF-8-DMBIM-PMPS membrane exhibited improved selectivity towards isobutanol while keeping the isobutanol flux (productivity) constant.

Figure S18.

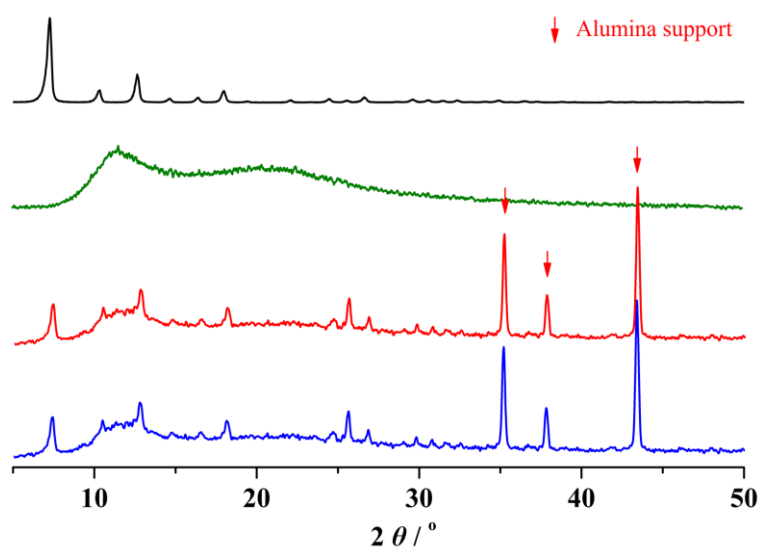


Figure S18. XRD patterns of ZIF-8-DMBIM nanocrystals (black), PMPS membrane (olive), ZIF-8-DMBIM-PMPS membrane as-synthesized (red) and after test for 24 h at 80 °C towards 3.0 wt.% isobutanol aqueous solution (blue).

The ZIF-8-DMBIM-PMPS membrane was endowed with good stability that no structure change of the membrane takes place after test for 24h (Figure S18), in virtue of the protection of the hydrophobic PMPS and DMBIM against water.